Supporting Information

Meinhold and Wright 10.1073/pnas.1105682108

SI Text

Protein Expression and Purification. Expression and purification of ^{1}H, ^{15}N-labeled wild-type apoMb was carried out as previously described (1, 2). Perdeuterated ^{2}H, ^{15}N-labeled protein was expressed in BL21 DE3 *Escherichia coli* cells that were acclimated to grow in 100% $^{2}H_2O$ media with ^{12}C, ^{2}H glucose and $(^{15}NH_4)_2SO_4$ as the sole carbon and nitrogen sources, respectively. Uniform ^{13}C labeling was accomplished by growing cells with ^{13}C glucose as the sole carbon source.

NMR Sample Preparation. Lyophilized protein was resuspended at a concentration of approximately 100 μM in 5 mM acetate buffer at pH 5.5, 4 °C. The samples were desalted using a Hi-Trap (GE Healthcare) gel filtration column in order to remove residual ionic contaminants from earlier steps of the purification. The samples were then concentrated to 650 μM and buffer exchanged to the appropriate pH necessary for each experiment, D_2O was added to reach a final concentration of 7%, and the samples were split in half for simultaneous data acquisition on two spectrometers.

Resonance Assignments. Backbone $^{1}H^{N}$, ^{15}N, and ^{13}CO resonances were assigned over the pH range 6.1–4.7 using a heteronuclear single quantum coherence (HSQC)-monitored pH titration to extrapolate assignments from those at pH 6.1 (3). Assignments were verified using a suite of 3D triple resonance experiments (4, 5) at pH 4.75. The ^{13}CO assignments were further confirmed using 3D HNCO spectra recorded at a series of pH values from 5.8 to 4.75.

R_2 Dispersion Analysis. Dispersion curves were generated by plotting the effective R_2 relaxation rate (R_2^{eff}) versus $1/\tau_{cp}$, where τ_{cp} is the spacing between the Carr–Purcell–Meiboom–Gill refocusing pulses, and R_2^{eff} is calculated from the spectral intensity with (I) and without (I_0) the constant-time relaxation delay as $-\ln(I/I_0)/T_{cp}$. Total constant-time relaxation (T_{cp}) delays were set as 40 and 80 ms for both single-quantum (SQ) ^{15}N and ^{13}CO, 30 and 60 ms for ^{1}H SQ, and 30 ms for zero-quantum (ZQ) and double-quantum (DQ) experiments. The 80- and 60-ms T_{cp} delays used in the SQ experiments allowed detection of R_2^{eff} below the lowest $1/\tau_{cp}$ frequency accessible with the 40- and 30-ms T_{cp} delays.

A two-state closed-form equation (6) was used to fit data from individual coherences (^{15}N, and ^{13}CO), whereas simultaneous two-state fitting of multiple coherences was accomplished using a numerical matrix formulation. Three-state modeling utilized a semianalytical expression for R_2^{eff} as a function of τ_{cp} (7), based on a generalized multisite solution (8). The largest eigenvalue of equation 4 from Sugase et. al. (7), substituted with the evolution matrix

$$A = \begin{pmatrix} R_{2A}^0 + k_{N,I1} + k_{N,MG} - i\Delta\omega_{I1,N}p & -k_{I1,N} & -k_{MG,N} \\ -k_{N,I1} & R_{2B}^0 + k_{I1,N} + k_{I1,MG} - i\Delta\omega_{N,I1}q & -k_{MG,I1} \\ -k_{N,MG} & -k_{I1,MG} & R_{2C}^0 + k_{MG,I1} + k_{MG,N} - i\Delta\omega_{N,MG}q - i\Delta\omega_{I1,MG}p \end{pmatrix}$$

yields R_2^{eff}, where $R_{2A}^0 = R_{2B}^0 = R_{2C}^0$. The parameterization of the three-state evolution matrix was selected as either ($p = 0, q = 1$: $\Delta\omega_{N,I1}$ and $\Delta\omega_{N,MG}$) or ($p = 1$, $q = 0$: $\Delta\omega_{I1,N}$ and $\Delta\omega_{I1,MG}$). Although both parameterization schemes were used at different stages of the optimization, the later scheme allowed for a better search of the complex local parameter space. The microscopic rates $k_{N,MG}$ and $k_{MG,N}$ were used to test for triangular connectivity of the three-state model, and were set to zero to generate a linear fitting model. In the case of modeling DQ and ZQ data, $\Delta\omega$ (rad s^{-1}) is equal to $\Delta\omega(^{1}H) + \Delta\omega(^{15}N)$ and $\Delta\omega(^{1}H) - \Delta\omega(^{15}N)$, respectively, for each of the two transitions.

Statistical comparison of fitting models was based on global χ^2 and Akaike information criterion (AIC) parameters (9). Comparisons were made between two- and three-state models, as well as the various configurations of the three-state model. The AIC parameter is expressed as

$$\text{AIC} = D\ln\left(\frac{S}{D}\right) + 2P + \frac{2P(P+1)}{D-P-1},$$

where D is the number of data points, S is the sum of squares, and P is the number of parameters plus one. The probability that the model with the lower AIC value is correct is expressed as a function of the difference in AIC between the two models (Δ):

$$\text{probability} = \frac{e^{-0.5\Delta}}{1 + e^{-0.5\Delta}}.$$

Fits to a model in which I1 is off-pathway lead to a 13 and 33% increase in global AIC and reduced χ^2 parameters, respectively, compared to the on-pathway (N ⇆ I1 ⇆ MG) model. Statistical tests thus strongly favor the on-pathway I1 model. In addition, fits to the off-pathway model yield unrealistically large $\Delta\omega_{N,I1}$ values ($^{1}H^{N} > 2$ ppm, and $^{15}N > 15$ ppm) for a subset of residues.

Model Optimization and Two-State Clustering. The parameter optimization protocol involved a succession of steps that were each accompanied and followed by global Levenberg–Marquardt (LM) optimization: (*i*) grid search of global parameter space, (*ii*) random sampling of global and local parameters, and (*iii*) Monte Carlo sampling. Global optimization of the three-state model of $^{1}H/^{15}N$ coherences required extensive randomization of local parameters $\Delta\omega_{A,B}$, and $\Delta\omega_{A,C}$. The additional randomization techniques made tentative changes to the local parameters, applied a limited number of LM iterations, and retained the final parameter set contingent upon lowering the value of χ^2. These steps play a significant role in circumventing barriers of local χ^2 minima predicted for three-state modeling of relaxation dispersion data (10). The first of the local randomization steps tested all possible permutations of the signs of each of the four $\Delta\omega$ parameters pertaining to ^{1}H and ^{15}N nuclei. The second local randomization step switched the values of $\Delta\omega_{A,B}$ and $\Delta\omega_{A,C}$ for each residue, both separately and simultaneously, for ^{1}H and ^{15}N nuclei. DQ and ZQ relaxation dispersion are dependent on the chemical shift differences of both nuclei in the spin system as $\Delta\omega = \Delta\omega(^{1}H) \pm \Delta\omega(^{15}N)$; thus, the relative

signs of $\Delta\omega(^1H)$ and $\Delta\omega(^{15}N)$ double the number of unique solutions. The results of local LM optimization after each trial were only retained if an improvement in χ^2 was realized.

A clustering algorithm was used to define groups of residues that exchange with similar kinetics. Initial clusters of ^{15}N relaxation dispersion curves (pH 4.75) were formed by fitting the entire ^{15}N relaxation dispersion dataset to a global two-state model and comparing the results of that fit to individual fits of each residue. Residues were removed from the global fit if the ratio $\chi^2_{Global}/\chi^2_{Individual}$ exceeded 2.0. This technique was applied recursively to the resultant cluster, as well as the new clusters formed by the rejected residues until all residues could be fit with a value of $\chi^2_{Cluster}$ less than double the value of $\chi^2_{Individual}$. The second step in clustering involved (*i*) identifying the core residues in each cluster, those with the highest data quality with R_{ex} values >4 s^{-1}, (*ii*) separately fitting the core residues in each cluster, and (*iii*) removing any of the remaining residues that could not be adequately fit using the rates and populations obtained solely from fits to the core residues. The final step incorporated an iterative process: (*i*) test the quality of fit of each residue with the kinetic parameters of each of the clusters, (*ii*) use the information from step (*i*) to move residues between clusters in order to reduce χ^2, (*iii*) optimize the kinetic parameters of the new clusters, and (*iv*) repeat steps (*i*) through (*iii*) until no further improvements could be made.

Initial Studies using ^{15}N SQ Relaxation with Nondeuterated apoMb. ^{15}N amide dispersion data acquired at pH 4.75, 35 °C using ^{15}N-labeled apoMb could not be adequately fit using a global two-state exchange mechanism. Local and clustered fitting of the kinetic exchange parameters were tested in order to account for the additional complexity that was not well fit by a global two-state model. Local two-state fitting coupled with Monte Carlo error analysis resulted in a broad spectrum of poorly defined kinetic exchange rates. Clustered two-state fits were completely ineffective at separating independent two-state events. The inadequacy of the clustered two-state model is strong evidence for a mechanism in which individual residues sample more than two conformational states. In order to overcome the inadequacy of the two-state model, a three-site exchange model was optimized to fit the amide data at pH 4.75. Simultaneous global fitting of data at multiple temperatures (30, 35, and 40 °C) assisted in parameter determination. Although the three-state model significantly improved the quality of fit over the two states, the three-state kinetic exchange rates were not well defined by the multiple-temperature SQ ^{15}N dispersion data alone.

Two-State Versus Three-State Fitting of SQ, DQ, and ZQ Data. The chemical shift parameters extracted from a global two-site exchange model unequivocally showed unfolding to a state that highly resembles the pH 4.1 molten globule (MG). Identification of the transient state as the MG intermediate was evident from the observed correlation between ($\Delta\omega$) the chemical shift differences (ω_{MG} : transient partially unfolded state) − (ω_N: ground-state) extracted from the fits of the R_2 dispersion data, and the absolute value of the chemical shift differences ($|\Delta\delta_{N,MG}|$) determined from HSQC and HNCO spectra under equilibrium conditions [pH 4.1, 50 °C, 10% EtOH (11) for MG, and pH 4.75, 35 °C for native (N)]. Although the correlation between $\Delta\omega$ and $\Delta\delta_{MG,N}$ suggests that some meaningful information can be extracted from the two-state model, 15% of the dataset is fit poorly by the global two-state model. Fitting to the three-state model leads to a 19 and 25% reduction in the global reduced χ^2 and AIC criterion, respectively.

The folding rates for the MG to N transition (250 s^{-1}) extracted from two-state fits (Table S1) to the amide dispersion data (^1H SQ, ^{15}N SQ, DQ, ZQ) were notably different from those determined by rapid-mixing kinetic experiments (20 s^{-1}) (12). The same data fitted to a three-state model yielded a folding rate (26 s^{-1}) close to that determined from the fast kinetics experiments, offering additional support for the use of a three-state model and underscoring the importance of modeling all significant transient states, including the highly native-like I1 state.

The magnitude of $\Delta\omega_{N,I1}$ is generally small in comparison to $\Delta\omega$ for the N to MG transition (Fig. S5), yet I1 has a relatively large population (9%) and thus has a significant effect on the shape of the dispersion curves. Even residues with very small $\Delta\omega_{N,I1}$ values display the effects of the N to I1 transition as an additional upward extension of R_2^{eff} in the lowest frequency ($1/\tau_{cp}$) region of the dispersion curve.

Three-State Fitting of $^{13}CO/^{15}N$ R_2 Dispersion at pH 4.75. A global two-state model yields moderate- to high-quality fits to ^{13}CO and ^{15}N datasets using a single set of exchange rates for both probes. A three-state model, however, yields a 30 and 70% reduction in global χ^2 and AIC values, respectively, while the main folding rate (MG → I1) is well determined by the three-state model (17 s^{-1}) and significantly overestimated (250 s^{-1}) by a two-state model (Table S1).

Global fitting of SQ ^{13}CO and ^{15}N R_2 dispersion data from a single sample required imposition of local parameter ($\Delta\omega_{N,I1}$) constraints to narrow the search for the three-state $\Delta\omega$ parameters. Because $\Delta\omega_{N,I1}$ at pH 4.75 showed close similarity to $\Delta\omega$ from pH 5.5 (Fig. S3), the $\Delta\omega$ parameters from two-state fits at pH 5.5 were used as constraints to fit the $^{15}N/^{13}CO$ data at pH 4.75. $\Delta\omega_{N,I1}$ parameters for both nuclei were bound to a range of ±20% of $\Delta\omega$ at pH 5.5 for all residues that yielded reliable $\Delta\omega$ values at pH 5.5. In contrast to the well-defined kinetic exchange rates extracted from the $^1H/^{15}N$ dataset, several combinations of the global kinetic rates were found to yield fits of similar quality to the $^{15}N/^{13}CO$ dataset. This uncertainty was quantified using a 10,000-point grid search of the kinetic parameter space. The starting conditions for LM optimization were varied through the apparent range of uncertainty for each of the global kinetic parameters. Full optimization for each set of starting conditions yielded a distribution of final parameter states and global χ^2 values that illustrated the degree of convergence and uncertainty for each parameter. The average and standard deviation of kinetic and $\Delta\omega$ parameters were extracted from the group of final parameters that yield high-quality global fits.

Comparison of Kinetic Models Using Data from Different Samples. Preliminary experiments showed that aliphatic deuteration increased the extent of unfolding at pH < 5 and made it necessary to increase the pH of a deuterated sample by 0.2 pH units above that of a nondeuterated sample in order to attain a similar magnitude of R_{ex}. As a result, ^{13}CO and amide dispersion data were recorded at different pH [4.75 and 4.95, respectively, for nondeuterated ($^{15}N/^{13}C$-labeled) and deuterated (^{15}N-labeled) apoMb samples]. The low buffering capacity of 5 mM acetate (the ionic strength must be kept low to limit the propensity of apoMb to aggregate) and the buffering capacity of apoMb itself at 600–700 μM also contribute to the challenge of obtaining reproducible R_{ex} values for independently prepared apoMb samples, even with the same isotope-labeling scheme. The equilibrium between the N and MG states is highly sensitive to pH and ionic strength at the edge of the unfolding transition (pH 4.75–4.95). As a result, minor variations in solution conditions have large effects on kinetic rate constants and the populations of the exchanging species. In order to address the question of whether the ^{13}C and amide probes monitor identical conformational exchange events, we acquired both sets of dispersion data on the same ($^{15}N/^{13}C$-labeled) sample and found that they were well fit using a single set of global three-state exchange kinetics.

Contribution of Intermolecular Interactions. The potential contribution of intermolecular interactions to the observed relaxation dispersion data was evaluated. N-state samples at or below 700 μM did not aggregate within the timeframe of the experiments, as evidenced by the lack of time-dependent changes in NMR peak intensities. Protein concentration dependence of R_{ex} was investigated by diluting a sample of pH 4.75 apoMb across a range of concentrations (600–300 μM). Because of the buffering capacity of apoMb in this concentration range, small pH corrections were necessary to account for a change in pH upon dilution. Given the high sensitivity of the N ⇆ MG equilibrium to pH and ionic strength, and the difference in ionic strength and buffering capacity between the 600- and 300-mM samples, the amplitude and pattern of R_{ex} between 600- and 300-μM samples are within reasonable agreement. The lack of significant concentration dependence of R_{ex} supports the use of a completely monomeric partial-unfolding model.

Dihedral Angle Analysis with TALOS+ Kinetic and $\Delta\omega$ parameters shown in Table 1 and Figs. 2 and 3 were extracted from a core set of the highest-quality relaxation dispersion curves characterized by significant R_{ex} and minimal random scatter in the dispersion curve. The remaining dispersion curves were analyzed to extract $\Delta\omega$ by fitting them to a constrained set of kinetics as defined by the higher-quality portion of the dataset. Excluding curves that are not analyzable because of excessive random scatter, or those that are extracted from peaks with significant overlap, all available $\Delta\omega$ parameters were included in the structural analysis of the transient MG state (Fig. 5). TALOS+ (13) was used to predict bond angles and secondary structure in the transient MG state. The chemical shifts used as input for TALOS+ were calculated with a combination of the N-state chemical shifts ($^1H^N$, ^{15}N, ^{13}CO), and $\Delta\omega_{N,MG}$ extracted from three-state relaxation dispersion analyses at pH 4.75–4.95 as described in Table S2.

Comparison of Transient and Equilibrium MGs. Within the limits of available secondary structure predictions, the segments of helical structure largely agree with TALOS+ (13) predictions of secondary structure in the pH 4.1 MG state, based on ^{15}N, $^1H^N$, $^1H_\alpha$, ^{13}CO, $^{13}C_\beta$, and $^{13}C_\alpha$ chemical shifts (11) (pH 4.1, 50 °C). The helical boundaries of the A, B, nonnative D–E, G, and H helices in the transient and pH 4.1 MG states are either identical (B, D–E, G, H) or one residue shorter (A) in the pH 4.1 MG. The C and E helices are shorter by two (42, 43) and three (68, 69, 70) residues, respectively, in the pH 4.1 MG. These small differences coincide with the lowest population and most dynamic helical structure, and they expose a minor pH-dependent plasticity in the boundaries of the MG-state helical structure. Salient differences exist between the populations of the predicted helical segments common between the two structures based on ^{13}CO chemical shifts. The population of helix in the transient MG state is on average 13% greater than that of the pH 4.1 MG state. This difference is reflected in a slope of 0.88 in the linear regression between $\Delta\omega_{N,MG}$ (^{13}CO) and $\Delta\delta_{N,MG}$ (^{13}CO) for residues in regions that are helical in both transient and pH 4.1 MG states. The chemical shifts depict an MG state that has minor and localized pH dependence of the helical segments.

1. Nishimura C, Dyson HJ, Wright PE (2006) Identification of native and non-native structure in kinetic folding intermediates of apomyoglobin. *J Mol Biol* 355:139–156.
2. Jennings PA, Stone MJ, Wright PE (1995) Overexpression of myoglobin and assignment of the amide, Cα and Cβ resonances. *J Biomol NMR* 6:271–276.
3. Eliezer D, Wright PE (1996) Is apomyoglobin a molten globule? Structural characterization by NMR. *J Mol Biol* 263:531–538.
4. Grzesiek S, Bax A (1992) Correlating backbone amide and side chain resonances in larger proteins by multiple relayed triple resonance NMR. *J Am Chem Soc* 114:6291–6293.
5. Grzesiek S, Bax A (1992) Improved 3D triple-resonance NMR techniques applied to a 31 kDa protein *J Magn Reson* 96:432–440.
6. Tollinger M, Skrynnikov NR, Mulder FA, Forman-Kay JD, Kay LE (2001) Slow dynamics in folded and unfolded states of an SH3 domain *J Am Chem Soc* 123:11341–11352.
7. Sugase K, Dyson HJ, Wright PE (2007) Mechanism of coupled folding and binding of an intrinsically disordered protein *Nature* 447:1021–1025.
8. Jen J (1978) Chemical exchange and Nmr T2 relaxation—Multisite case. *J Magn Reson* 30:111–128.
9. Motulsky H, Christopoulos A (2004) *Fitting Models to Biological Data Using Linear and Nonlinear Regression: A Practical Guide to Curve Fitting* (Oxford Univ Press, Oxford).
10. Neudecker P, Korzhnev D, Kay L (2006) Assessment of the effects of increased relaxation dispersion data on the extraction of 3-site exchange parameters characterizing the unfolding of an SH3 domain. *J Biomol NMR* 34:129–135.
11. Eliezer D, Chung J, Dyson HJ, Wright PE (2000) Native and non-native structure and dynamics in the pH 4 intermediate of apomyoglobin. *Biochemistry* 39:2894–2901.
12. Uzawa T, et al. (2004) Collapse and search dynamics of apomyoglobin folding revealed by submillisecond observations of α-helical content and compactness *Proc Natl Acad Sci USA* 101:1171–1176.
13. Shen Y., Delaglio F, Cornilescu G, Bax A (2009) TALOS+: A hybrid method for predicting protein backbone torsion angles from NMR chemical shifts. *J Biomol NMR* 44: 213–223.

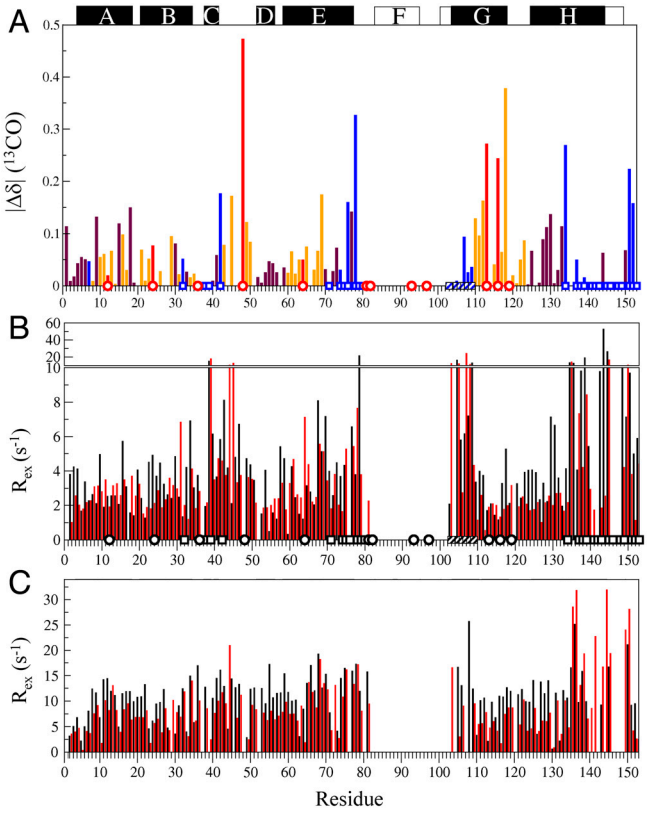

Fig. S1. pH dependence of the N-state ensemble and conformational exchange at pH 5.5. (*A*) Absolute values of ^{13}CO chemical shift differences ($\Delta\delta$, ppm) between pH 5.8 and 4.75 measured using 3D HNCO experiments. Open squares and blue bars depict the locations of contacts to the F helix and the first 1.5 turns of the G helix (residues 82–104), whereas the hashed squares represent the residues at the N terminus of G, which flank the F helix and the F–G loop. Circles and red bars highlight the location of His residues, and orange bars highlight the location of contacts with His residues. All other residues are colored purple. The largest chemical shift changes are associated with protonation of His side chains and a shift in the F-helix conformational ensemble. The locations of the helices in native apoMb, derived using TALOS+ (13) with $^{1}H^{N}$, ^{15}N, ^{13}CO, $^{13}C^{\alpha}$, $^{1}H^{\alpha}$ chemical shifts (3), are indicated by black filled rectangles, whereas the boundaries of the F, G, and H helices in holoMb are shown by open rectangles. (*B*) Comparison of ^{15}N (red) and ^{13}CO (black) R_{ex} (500 MHz) at pH 5.5 shows that the two probes yield highly similar patterns in which the most pronounced exchange effects are localized around the regions that contact the F helix and the N terminus of the G helix. The open/hashed squares and circles below *B* are defined as in *A*. R_{ex} values determined for apoMb at pH < 5.0 (35 °C). (*C*) ^{15}N R_{ex} values for perdeuterated apoMb at pH 4.95 are shown as red bars, and values for protonated ^{15}N/^{13}C-labeled apoMb at pH 4.75 are shown as black bars. These samples were used to acquire the dispersion data shown in Figs. 2 and 3, respectively. The differences in sample composition cause the protonated sample to populate the MG state to a slightly larger extent, giving higher values of R_{ex}.

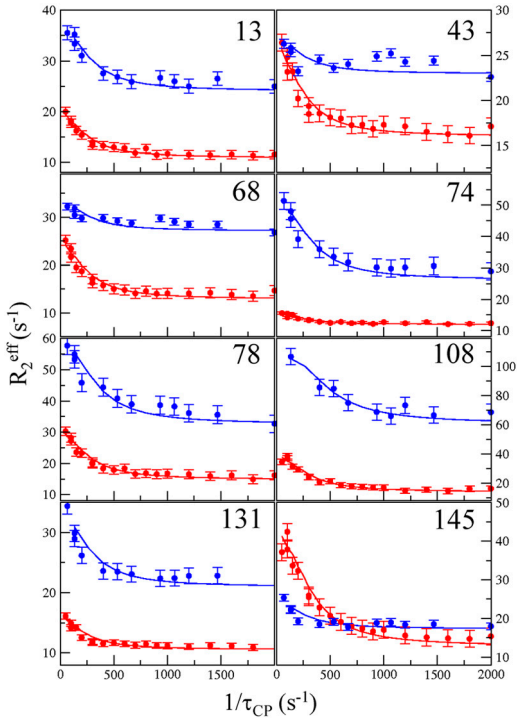

Fig. S2. Representative ^{15}N (red) and ^{1}H (blue) relaxation dispersion profiles at a static magnetic field of 18.8 T acquired on perdeuterated ^{15}N apoMb at pH 5.5. Data obtained at two static magnetic fields (11.7 and 18.8 T) were used in a clustered fit of all residues within the contacts sites of the F helix and the first helical turn of G; residues that exhibited dispersion in the ranges 39–45, 72–81, 103–109, 141–153 were used in the fits. The fits to a two-state exchange model are shown as lines. The kinetic parameters are summarized in Table 1.

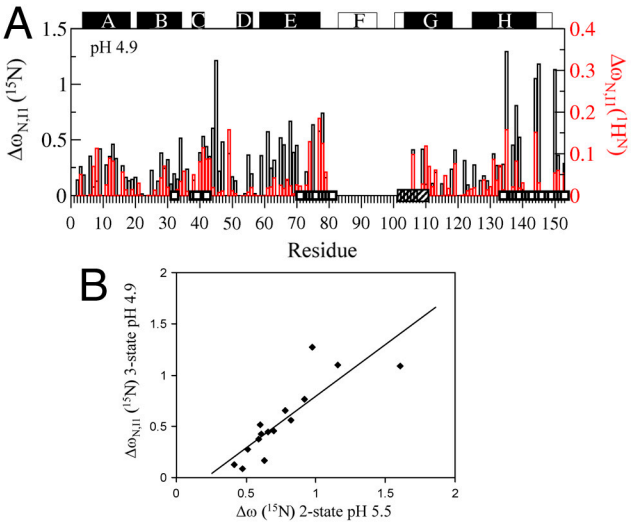

Fig. S3. The transient state formed at pH 5.5 is similar to the I1 state at pH 4.95. (*A*) Chemical shift differences (ppm) between N and I1 ($|\Delta\omega_{N,I1}|$) extracted from a three-state global fit to the four types of amide R_2 dispersion curves at pH 4.9, 35 °C plotted against residue number. $\Delta\omega$ (^{15}N) values (black) are plotted along the left *y* axis, and the right axis shows $\Delta\omega$ ($^{1}H^N$) (red). The open and hashed squares at the bottom of the plot are as defined in Fig. S1. (*B*) Correlation plot between $\Delta\omega$ extracted from a two-state fit to the clustered data at pH 5.5, and $\Delta\omega_{N,I1}$ extracted from a three-state global fit to data at pH 4.95. The clustered fit includes residues 39–45, 72–81, 103–109, 141–153, which are in F helix or FG loop contact sites. The solid line shows a linear fit yielding the expression: $y = x - 0.2$. Although the slope shows that the pattern of chemical shifts between the two pH conditions is very similar, the *y*-axis offset of −0.2 ppm is likely due to the presence of a small population of the MG state at pH 5.5, which is not accounted for by the two-state model. The bars at the top of the figure represent helical boundaries as defined in Fig. S1.

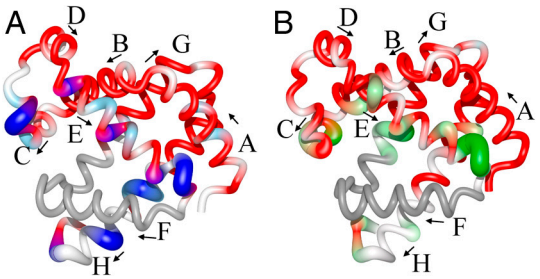

Fig. S4. Amide and ^{13}CO chemical shift differences ($\Delta\omega$) between the native and transient I1 states derived from three-state fits to relaxation dispersion data at pH 4.75 (^{13}CO) and 4.95 (amide). (*A*) ^{15}N $\Delta\omega_{N,I1}$ shifts mapped to the structure of holoMb (Protein Data Bank ID code 1MBC). Values of $\Delta\omega_{N,I1}$ greater than the mean are colored blue; the amplitude is indicated by tube thickness and color saturation. The gray tubes represent the F helix and the first turn of the G helix, and the white tubes represent regions that are associated with resonances that are either broadened beyond detection or that yield R_2 dispersion curves that are too noisy to fit. (*B*) ^{13}CO $\Delta\omega_{N,I1}$ shifts mapped to the structure using the same scheme as in *A* except that green is used for values greater than the mean. This figure was prepared using MolMol (1).

1 Koradi R, Billeter M, Wüthrich K (1996) MOLMOL: A program for display and analysis of macromolecular structures. *J Mol Graph* 14:51–55.

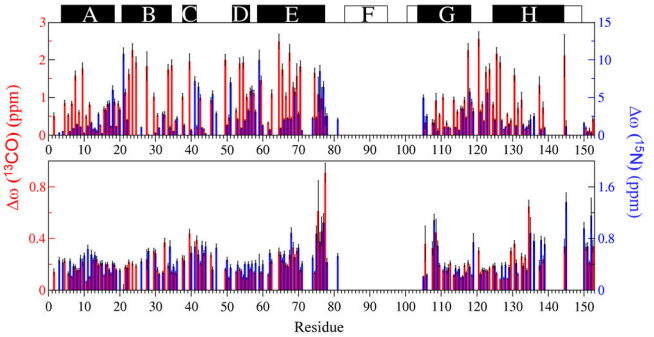

Fig. S5. The absolute value of $\Delta\omega$ obtained from simultaneous fits to ^{13}CO (red) and ^{15}N (blue) R_2 dispersion curves acquired on ^{1}H/^{15}N/^{13}C-labeled apoMb at pH 4.75, 35 °C. $\Delta\omega$ values for the N ⇆ MG and N ⇆ I1 transitions are shown in *A* and *B*, respectively. Parameters and error bars were determined as described in *SI Text*. The bars at the top of the figure represent helical boundaries as defined in Fig. S1.

Table S1. Kinetic parameters from a two-state analysis of apoMb transient unfolding and refolding

Probe	K_{ex}, s^{-1}	$k_{N,MG}$, s^{-1}	$k_{MG,N}$, s^{-1}	P_N	P_{MG}
^{15}N/^{1}H*	441 ± 16	27 ± 3	414 ± 16	0.94 ± 0.05	0.06 ± 0.01
^{13}CO/^{15}N†	270 ± 20	14 ± 1	250 ± 20	0.95 ± 0.00	0.05 ± 0.00

*Parameters from a two-state fit to R_2 relaxation dispersion data as shown in Fig. 2 (pH 4.95, 35 °C) using four types of amide coherences (^{1}H-SQ, ^{15}N-SQ, ^{1}H/^{15}N-DQ, ^{1}H/^{15}N-ZQ). Uncertainty was determined using Monte Carlo sampling.

†Parameters from a two-state global fit to ^{13}CO and ^{15}N R_2 relaxation dispersion data shown in Fig. 3 (pH 4.75, 35 °C). Uncertainty was determined using Monte Carlo sampling.

Table S2. ^{15}N chemical shifts (ppm) derived from three-state global fits to four types of amide relaxation dispersion curves (SQ-^{1}H, SQ-^{15}N, ZQ, DQ) acquired for perdeuterated apoMb at pH 4.95, 35 °C

Residue no.	$\lvert\Delta\omega_{N,MG}(^{15}N)\rvert$*	Error*	$\lvert\Delta\omega_{N,I1}(^{15}N)\rvert$*	Error*	Data quality*	ω_N† pH 4.95, 35 °C	$\Delta\delta_{N,MG}$ (^{15}N)‡ (pH 4.95, 35 °C)–(pH 4.1, 50 °C)	ω_{TrMG}^{15N}§
2	0.23	0.02	0.24	0.00	S	125.20	0.10	125.35
3	0.31	0.03	0.26	0.03	K	118.14	0.92	118.22
4	0.57	0.04	0.18	0.02	K	121.02	−0.70	121.97
5	0.00	0.03	0.20	0.00	S	106.26	−0.46	106.64
6	0.05	0.10	0.35	0.06	K	122.64	1.29	122.96
7	0.91	0.07	0.08	0.05	K	118.95	−0.90	120.24
8	1.05	0.06	0.13	0.04	K	116.55	0.46	115.88
9	0.57	0.09	0.42	0.02	K	119.48	−0.74	120.43
10	0.79	0.00	0.19	0.00	S	119.05	0.32	118.63
11	1.49	0.21	0.27	0.03	K	119.06	0.72	117.96
12	2.32	0.05	0.35	0.04	K	119.35	2.50	117.40
13	2.01	0.45	0.46	0.03	K	117.52	−1.57	119.91
14	3.05	0.37	0.33	0.02	K	122.87	2.27	120.19
15	0.51	0.06	0.00	0.17	K	118.10	−1.00	118.98

Residue no.	$\lvert\Delta\omega_{N,MG}(^{15}N)\rvert$*	Error*	$\lvert\Delta\omega_{N,I1}(^{15}N)\rvert$*	Error*	Data quality*	ω_N† pH 4.95, 35 °C	$\Delta\delta_{N,MG}$ (^{15}N)‡ (pH 4.95, 35 °C)–(pH 4.1, 50 °C)	ω^{15N}_{TrMG}§
16	3.48	0.36	0.27	0.04	K	114.31	−2.91	118.17
17	3.67	0.15	0.16	0.03	K	120.85	2.50	117.56
18	6.46	0.61	0.13	0.09	K	114.45	−5.00	121.28
19	1.28	0.66	0.15	0.00	S	119.09	−1.88	120.76
20	3.58	0.15	0.16	0.05	K	115.34	−2.63	119.30
21	10.01	0.33	0.00	0.05	K	130.05	12.08	120.43
22	2.27	0.07	0.01	0.02	K	121.64	−1.96	124.29
23	0.09	0.00	0.19	0.00	S	105.78	−0.57	106.24
24	0.99	0.05	0.00	0.00	K	116.52	−0.70	117.89
25	0.88	0.02	0.23	0.04	K	107.94	−0.65	109.21
26	0.63	0.03	0.00	0.00	K	119.71	0.23	119.46
27	2.03	0.28	0.31	0.02	K	117.44	−1.66	119.85
28	0.23	0.08	0.38	0.02	K	119.19	0.09	119.34
29	1.25	0.10	0.25	0.04	K	118.46	−1.77	120.08
30	0.44	0.08	0.32	0.06	K	117.76	0.54	117.70
31	0.74	0.03	0.10	0.04	K	117.91	−0.81	119.02
32	2.51	0.16	0.20	0.03	K	122.19	2.34	120.06
33	0.27	0.02	0.15	0.02	K	116.44	−0.41	117.09
34	2.61	0.33	0.51	0.03	K	117.07	−1.28	120.06
35	0.88	0.05	0.00	0.01	K	112.97	−0.12	114.23
36	1.90	0.08	0.24	0.03	K	116.98	−1.37	119.26
38	1.21	0.06	0.14	0.02	K	121.59	0.99	120.75
39	0.74	0.00	1.30	0.00	S	114.08	−0.52	115.20
40	0.60	0.19	0.38	0.05	K	122.51	0.42	122.29
41	6.26	0.56	0.53	0.01	K	113.51	−5.58	120.15
42	6.50	0.43	0.44	0.04	K	114.19	−4.90	121.07
43	2.69	0.17	0.35	0.05	K	120.35	1.26	118.04
44	4.82	0.37	0.60	0.04	K	122.08	1.11	117.64
45	7.20	1.29	1.21	0.05	K	115.90	−3.94	123.48
46	7.68	0.37	0.22	0.01	K	114.02	−3.95	122.08
47	3.66	0.17	0.48	0.01	K	117.20	−2.65	121.23
49	0.30	0.12	0.30	0.00	S	122.36	−0.12	123.04
50	0.49	0.05	0.17	0.08	K	120.01	−1.33	120.89
51	5.19	0.18	0.13	0.01	K	107.48	−5.99	113.05
53	2.41	0.05	0.00	0.00	K	120.09	−2.38	122.88
54	1.40	0.03	0.02	0.01	K	117.75	−0.60	119.53
55	1.51	0.29	0.27	0.00	S	118.26	−1.96	120.15
56	3.76	0.26	0.20	0.02	K	117.92	−2.68	122.06
57	5.16	0.33	0.02	0.04	K	117.77	−5.07	123.32
58	2.67	0.25	0.00	0.00	K	111.05	−2.42	114.10
59	10.79	0.41	0.36	0.08	K	134.48	12.76	124.07
60	1.01	0.08	0.00	0.09	K	118.76	−1.09	120.15
61	4.87	0.27	0.57	0.02	K	123.38	2.41	118.88
62	1.06	0.09	0.25	0.03	K	119.62	0.89	118.93
63	1.07	0.07	0.31	0.04	K	117.82	−0.90	119.27
64	0.03	0.00	0.89	0.00	S	120.26	3.04	120.61
65	1.83	0.31	0.52	0.03	K	107.83	−1.14	110.04
66	2.01	0.07	0.45	0.03	K	120.89	2.16	119.25
67	3.92	0.16	0.14	0.03	K	120.47	2.87	116.92
68	3.04	0.29	0.67	0.02	K	120.67	−1.05	124.09
69	5.91	0.43	0.39	0.02	K	116.84	−6.38	123.13
70	2.33	0.21	0.45	0.01	K	116.62	2.40	114.67
71	0.65	0.07	0.03	0.05	K	124.72	−0.38	125.75
72	1.78	0.00	0.79	0.14	S	117.47	−1.62	119.64
73	0.00	0.02	0.21	0.01	K	106.97	−0.13	107.35
74	2.14	0.25	0.00	0.01	K	120.70	−1.77	123.22
75	1.81	0.22	0.63	0.01	K	116.25	−1.34	118.44
77	7.08	0.57	0.58	0.04	K	113.47	−6.38	120.94
78	4.20	0.09	0.74	0.04	K	115.90	−4.69	120.48
79	3.85	0.27	0.16	0.03	K	118.71	−2.64	122.94
103	2.84	0.00	1.10	0.00	S	115.89	−2.46	119.11
105	4.57	0.27	0.49	0.06	S	123.15	3.30	118.96
106	3.91	0.46	0.41	0.01	K	118.33	−0.76	122.62
107	4.27	0.00	2.26	0.00	S	121.25	2.53	117.37
108	0.82	0.00	1.21	0.00	S	116.92	1.20	116.48
109	1.00	0.07	0.42	0.01	K	120.24	0.39	119.62
110	1.07	0.36	0.10	0.08	K	121.95	−0.14	123.41
111	0.67	0.04	0.01	0.01	K	117.71	0.87	117.42
112	0.86	0.03	0.11	0.07	K	118.42	−1.06	119.65
113	2.57	0.43	0.21	0.02	K	117.30	0.08	115.11
114	1.45	0.05	0.00	0.00	K	120.13		

Residue no.	$\lvert\Delta\omega_{N,MG}(^{15}N)\rvert$*	Error*	$\lvert\Delta\omega_{N,I1}(^{15}N)\rvert$*	Error*	Data quality*	ω_N† pH 4.95, 35 °C	$\Delta\delta_{N,MG}$ (^{15}N)‡ (pH 4.95, 35 °C)–(pH 4.1, 50 °C)	ω_{TrMG}^{15N}§
115	0.56	0.03	0.11	0.06	K	120.03	−0.19	120.96
116	0.14	0.02	0.00	0.00	K	115.25	−0.47	115.77
117	2.92	0.15	0.00	0.08	K	112.39	−2.21	115.69
118	4.88	0.18	0.24	0.02	K	115.60	−5.00	120.86
119	4.01	0.59	0.41	0.03	K	114.81	−3.92	119.20
121	2.62	0.07	0.00	0.00	K	106.09	−2.50	109.09
122	3.66	0.18	0.13	0.07	K	117.22	−2.25	121.26
123	0.04	0.06	0.10	0.03	K	123.12	3.27	123.46
124	0.72	0.04	0.06	0.04	K	109.53	0.56	109.19
125	0.33	0.02	0.27	0.01	K	120.98	−1.87	121.69
126	0.59	0.02	0.00	0.00	K	117.35	−0.25	118.32
127	1.08	0.04	0.13	0.04	K	126.12	2.14	125.42
128	1.06	0.12	0.18	0.03	K	118.23	1.01	117.54
129	1.77	0.18	0.13	0.02	K	106.59	−1.63	108.74
130	0.17	0.00	0.00	0.00	K	124.10	0.50	124.30
131	0.87	0.09	0.37	0.03	K	116.69	−0.90	117.94
132	0.35	0.09	0.27	0.04	K	117.67	−0.30	118.39
133	1.24	0.06	0.26	0.01	K	119.01	−1.21	120.63
134	0.06	0.06	0.28	0.02	K	121.76	0.03	122.07
135	2.32	0.54	0.92	0.00	S	115.77	−1.83	118.47
136	1.24	0.00	1.19	0.00	S	120.72	1.62	119.86
137	2.38	0.30	0.45	0.04	K	120.53	1.06	118.53
138	6.10	0.24	0.81	0.04	K	117.61	−1.11	124.09
139	0.16	0.04	0.52	0.03	K	120.25	1.53	120.48
140	0.36	0.04	0.05	0.02	K	120.91	1.82	120.93
141	1.26	0.00	0.19	0.00	S	120.00	0.53	119.11
144	2.61	0.39	1.05	0.07	K	118.91	−0.19	121.89
145	0.55	0.40	1.18	0.05	K	119.82	2.22	119.64
149	2.89	0.00	0.76	0.00	S	117.94	−1.16	121.21
150	1.70	1.11	1.13	0.08	K	106.08	−1.01	108.16
151	0.36	0.00	0.36	0.01	K	119.98	0.51	120.00
153	0.04	0.03	0.29	0.01	K	115.28	0.68	115.61

*Values of $\Delta\omega_{N,MG}$ and $\Delta\omega_{N,I1}$ were obtained by fitting the relaxation dispersion data to the three-state model N ⇆ I1 ⇆ MG. The two types of data quality reported in the table correspond to high-quality datasets (K) used in the determination of global three-state kinetic parameters, and (S) those that were incorporated into inferences about the structural content of the transient MG state but were not used to determine global kinetics. Parameters labeled with "S" were extracted from R_2 dispersion curves that exhibited excessive scatter in one or more of the SQ-^{1}H, SQ-^{15}N, ZQ, DQ R_2^{eff} vs $1/tcp$ profiles or small R_{ex} values. In order to extract $\Delta\omega$ parameters from the lower-quality datasets, the global kinetic rates were held constant to the values shown in Table 1, which were obtained from fits to the high-quality data (K). Uncertainties for the higher-quality data were determined using Monte Carlo sampling, whereas those associated with lower-quality data were determined from the covariance matrix of a single fit with kinetic parameters constrained as described above. The uncertainties of the lower-quality data are, therefore, significantly underestimated.

†ω_N represents the (^{15}N) chemical shift of native apoMb measured under identical sample conditions (pH 4.95, 35 °C) as those used to acquire relaxation dispersion data summarized by the chemical shifts in the table. Chemical shift assignments were transferred from published assignments at pH 6.1 (3) and verified as described in *Materials and Methods*. Chemical shift referencing is indirectly based on DSS (5,5-dimethylsilapentanesulfonate).

‡$\Delta\delta_{N,MG}$ was calculated as the difference between the native state (designated ω_N) and published MG-state chemical shifts (11), all referenced to DSS.

§ω_{TrMG}^{15N} is the chemical shift of the transient MG state calculated from the native-state chemical shift (ω_N), $\Delta\omega_{N,MG}$, and $\Delta\delta_{N,MG}$ ($\omega_{TrMG}^{15N} = \omega_N$-sign($\Delta\delta_{N,MG}$)$\lvert\Delta\omega_{N,MG}\rvert$), where it is assumed that the sign of $\Delta\omega_{N,MG}$ is the same as that of $\Delta\delta_{N,MG}$. This assumption is supported by the strong linear correlation between the magnitudes of $\Delta\omega_{N,MG}$ and $\Delta\delta_{N,MG}$ (Figs. 2 and 3) for three nuclei ($^1H^N$, ^{15}N, ^{13}CO).

Table S3. $^1H^N$ chemical shifts (ppm) derived from three-state global fits to four types of amide relaxation dispersion curves (SQ-^{1}H, SQ-^{15}N, ZQ, DQ) acquired for perdeuterated apoMb at pH 4.95, 35 °C

Residue no.	$\lvert\Delta\omega_{N,MG}(^1H^N)\rvert$*	Error*	$\lvert\Delta\omega_{N,I1}(^1H^N)\rvert$*	Error*	Data quality*	ω_H† pH 4.95, 35 °C	$\Delta\delta_{N,MG}$ ($^1H^N$)‡ (pH 4.95, 35 °C)–(pH 4.1, 50 °C)	ω_{TrMG}^{1HN}§
2	0.00	0.00	0.01	0.01	S	8.16	0.15	8.26
3	0.09	0.01	0.05	0.00	K	9.06	0.73	9.07
4	0.10	0.00	0.00	0.00	K	9.03	0.35	9.02
5	0.02	0.02	0.01	0.01	S	8.58	0.18	8.67
6	0.03	0.00	0.00	0.00	K	7.71	−0.04	7.84
7	0.16	0.01	0.07	0.00	K	8.56	0.32	8.50
8	0.07	0.02	0.11	0.00	K	8.23	0.26	8.25
9	0.20	0.01	0.00	0.00	K	7.52	0.14	7.43
10	0.00	0.00	0.00	0.00	S	7.91	0.16	8.01
11	0.86	0.02	0.03	0.00	K	8.85	0.88	8.09
12	0.31	0.01	0.09	0.00	K	8.34	0.47	8.13
13	0.36	0.03	0.08	0.00	K	7.60	−0.40	8.07
14	0.29	0.01	0.00	0.00	K	8.87	0.48	8.67
15	0.40	0.01	0.00	0.00	K	7.51	−0.39	8.01
16	0.43	0.09	0.06	0.00	K	6.97	−0.41	7.50
17	1.32	0.06	0.01	0.00	K	6.66	−1.09	8.07
18	0.67	0.05	0.00	0.00	K	7.35	−0.39	8.12

Residue no.	$\lvert\Delta\omega_{N,MG}(^1H^N)\rvert$*	Error*	$\lvert\Delta\omega_{N,I1}(^1H^N)\rvert$*	Error*	Data quality*	ω_H† pH 4.95, 35 °C	$\Delta\delta_{N,MG}$ ($^1H^N$)‡ (pH 4.95, 35 °C)–(pH 4.1, 50 °C)	$\omega_{TrMG}^{^1H^N}$§
19	0.85	0.05	0.02	0.00	S	6.68	−0.83	7.63
20	0.32	0.02	0.00	0.01	K	7.50	−0.31	7.92
21	1.17	0.07	0.03	0.00	K	8.81	1.06	7.74
22	0.45	0.01	0.00	0.00	K	8.49	0.59	8.14
23	0.05	0.01	0.00	0.01	S	8.05	0.12	8.10
24	0.51	0.01	0.00	0.00	K	7.61	−0.46	8.22
25	0.24	0.01	0.00	0.00	K	8.76	0.40	8.62
26	0.19	0.01	0.01	0.00	K	8.02	−0.14	8.31
27	0.55	0.02	0.00	0.00	K	7.51	−0.60	8.16
28	0.61	0.06	0.04	0.00	K	8.27	0.63	7.76
29	0.29	0.03	0.07	0.00	K	7.48	−0.11	7.86
30	0.24	0.01	0.02	0.00	K	8.17	0.56	8.02
31	0.03	0.00	0.00	0.00	K	7.61	0.09	7.69
32	0.17	0.01	0.01	0.01	K	7.98	0.24	7.91
33	0.19	0.00	0.01	0.00	K	8.15	0.34	8.05
34	0.54	0.03	0.03	0.00	K	8.31	0.56	7.86
35	0.14	0.01	0.06	0.00	K	7.96	0.26	7.92
36	0.05	0.00	0.01	0.00	K	8.05	0.06	8.10
38	1.41	0.07	0.05	0.00	K	10.33	1.21	9.02
39	0.51	0.00	0.04	0.00	S	8.28	0.43	7.87
40	0.40	0.02	0.08	0.00	K	7.29	−0.31	7.79
41	0.70	0.06	0.11	0.00	K	7.30	−0.52	8.10
42	0.75	0.05	0.09	0.00	K	7.28	−0.38	8.13
43	0.15	0.02	0.09	0.01	K	7.74	−0.01	7.99
44	0.34	0.04	0.02	0.00	K	8.06	0.06	7.82
45	0.28	0.06	0.00	0.00	K	8.25	0.41	8.07
46	0.79	0.04	0.01	0.00	K	7.38	−0.42	8.26
47	0.41	0.02	0.01	0.00	K	7.33	−0.38	7.84
49	0.25	0.00	0.39	0.00	S	7.54	−0.33	7.90
50	0.13	0.01	0.01	0.01	K	8.31	0.28	8.27
51	0.44	0.02	0.00	0.00	K	7.61	−0.22	8.14
53	0.12	0.00	0.00	0.00	K	8.26	0.29	8.25
54	0.24	0.00	0.00	0.00	K	7.66	−0.19	7.99
55	0.09	0.05	0.01	0.01	S	8.04	0.06	8.05
56	0.29	0.01	0.02	0.00	K	8.38	0.44	8.19
57	0.87	0.03	0.00	0.00	K	7.08	−0.79	8.04
58	1.11	0.04	0.00	0.00	K	6.84	−1.00	8.05
59	1.09	0.04	0.00	0.00	K	9.21	1.22	8.22
60	0.05	0.00	0.00	0.00	K	8.22	0.18	8.27
61	0.59	0.02	0.02	0.00	K	8.17	0.38	7.68
62	0.57	0.02	0.02	0.00	K	7.31	−0.43	7.99
63	0.46	0.06	0.04	0.00	K	8.26	0.57	7.90
64	0.00	0.40	0.00	0.14	S	8.16	0.19	8.26
65	0.26	0.03	0.02	0.00	K	8.47	0.38	8.31
66	0.08	0.00	0.02	0.00	K	7.95	0.15	7.97
67	0.49	0.02	0.04	0.00	K	8.26	0.31	7.87
68	0.14	0.01	0.02	0.00	K	8.07	0.20	8.03
69	0.17	0.01	0.00	0.00	K	7.95	0.00	8.22
70	0.63	0.02	0.03	0.00	K	8.73	0.97	8.20
71	0.43	0.03	0.02	0.00	K	7.59	−0.32	8.12
72	0.74	0.03	0.15	0.03	S	7.84	−0.02	8.68
73	0.64	0.03	0.02	0.00	K	8.63	0.64	8.09
74	0.15	0.03	0.13	0.00	K	7.47	−0.19	7.72
75	0.68	0.02	0.00	0.00	K	6.96	−0.63	7.74
77	0.21	0.34	0.18	0.02	K	7.86	0.15	7.75
78	0.48	0.02	0.12	0.00	K	6.88	−0.86	7.46
79	0.33	0.02	0.06	0.00	K	7.66	−0.31	8.09
103	0.18	0.00	0.46	0.00	S	7.42	−0.08	7.69
105	0.46	0.00	0.00	0.00	S	8.07	−0.03	8.63
106	0.28	0.03	0.10	0.00	K	7.66	0.01	7.48
107	0.54	0.00	0.09	0.00	S	8.62	0.72	8.18
108	0.10	0.00	0.45	0.00	S	7.82	0.00	8.02
109	0.26	0.01	0.03	0.00	K	7.73	−0.10	8.09
110	0.05	0.02	0.12	0.01	K	7.73	−0.05	7.88
111	0.13	0.04	0.07	0.01	K	8.33	0.54	8.30
112	0.04	0.01	0.02	0.00	K	7.82	0.11	7.89
113	0.48	0.04	0.06	0.00	K	8.18	0.29	7.80
114	0.49	0.01	0.00	0.00	K	8.42		
115	0.56	0.03	0.00	0.00	K	8.48	0.53	8.02
116	0.02	0.01	0.05	0.00	K	8.01	0.13	8.09
117	0.26	0.01	0.02	0.00	K	7.93	0.30	7.76

Residue no.	$\lvert\Delta\omega_{N,MG}(^1H^N)\rvert$*	Error*	$\lvert\Delta\omega_{N,I1}(^1H^N)\rvert$*	Error*	Data quality*	ω_H† pH 4.95, 35 °C	$\Delta\delta_{N,MG}$ ($^1H^N$)‡ (pH 4.95, 35 °C)–(pH 4.1, 50 °C)	$\omega_{TrMG}^{^1H^N}$§
118	0.46	0.01	0.00	0.00	K	8.14	0.26	7.77
119	1.09	0.22	0.08	0.00	K	7.42	−0.72	8.61
121	0.05	0.00	0.00	0.00	K	8.47	0.21	8.52
122	0.37	0.01	0.00	0.00	K	7.46	−0.29	7.94
123	0.15	0.01	0.01	0.00	K	7.87	−0.10	8.11
124	0.17	0.01	0.02	0.00	K	7.99	−0.05	8.26
125	0.03	0.00	0.02	0.00	K	8.42	0.45	8.49
126	0.28	0.01	0.00	0.00	K	8.49	0.39	8.31
127	0.05	0.00	0.00	0.00	K	8.14	0.19	8.19
128	0.17	0.01	0.04	0.00	K	8.33	0.25	8.26
129	0.23	0.02	0.01	0.00	K	7.93	−0.19	8.27
130	0.40	0.01	0.02	0.00	K	7.62	−0.27	8.12
131	0.38	0.02	0.09	0.00	K	8.50	0.46	8.22
132	0.31	0.01	0.04	0.00	K	8.50	0.47	8.29
133	0.30	0.03	0.07	0.00	K	7.47	−0.38	7.86
134	0.14	0.01	0.01	0.00	K	8.10	0.21	8.05
135	0.15	0.00	0.23	0.00	S	8.48	0.55	8.43
136	0.19	0.00	0.24	0.00	S	7.66	−0.09	7.95
137	0.05	0.03	0.02	0.00	K	7.83	0.10	7.88
138	0.59	0.02	0.08	0.00	K	7.78	−0.19	8.46
139	0.20	0.01	0.02	0.00	K	7.76	−0.28	8.06
140	0.14	0.01	0.03	0.00	K	8.31	0.45	8.26
141	0.06	0.00	0.05	0.00	S	7.93	−0.07	8.09
144	1.47	0.33	0.15	0.02	K	7.52	−0.05	9.09
145	0.11	0.02	0.03	0.00	K	8.17	0.54	8.16
149	0.19	0.00	0.17	0.00	S	7.72	0.03	7.63
150	0.90	0.19	0.05	0.01	K	7.81	0.00	7.01
151	0.21	0.01	0.06	0.00	K	7.84	0.20	7.73
153	0.70	0.12	0.05	0.00	K	7.31	0.06	6.71

*Values of $\Delta\omega_{N,MG}$ and $\Delta\omega_{N,I1}$ ($^1H^N$), uncertainties, and data-quality designations are as described in Table S2.
†ω_H represents the ($^1H^N$) chemical shift of native apoMb as described in Table S2.
‡$\Delta\delta_{N,MG}$ was calculated as described in Table S2.
§$\omega_{TrMG}^{^1H^N}$ is the chemical shift of the transient MG state calculated as described in Table S2.

Table S4. ^{13}CO chemical shifts (ppm) derived from simultaneous three-state global fits to ^{13}CO and ^{15}N relaxation dispersion curves acquired for protonated apoMb at pH 4.75, 35 °C

Residue no.	$\lvert\Delta\omega_{N,MG}(^{13}CO)\rvert$*	Error*	$\lvert\Delta\omega_{N,I1}(^{13}CO)\rvert$*	Error*	Data quality*	ω_{CO}† pH 4.95, 35 °C	$\Delta\delta_{N,MG}$ (CO)‡ (pH 4.75, 35 °C)–(pH 4.1, 50 °C)	$\omega_{TrMG}^{^{13}CO}$§
1	0.51	0.09	0.14	0.03	K	174.82	−0.18	175.41
2	0.02	0.00	0.20	0.00	S	176.83	0.19	176.91
3	0.01	0.00	0.20	0.00	S	174.95	0.03	175.01
4	0.85	0.08	0.23	0.02	K	179.53	1.19	178.77
5	0.53	0.04	0.13	0.02	K	177.33	1.06	176.89
6	0.84	0.07	0.10	0.01	K	178.93	0.95	178.18
7	1.58	0.13	0.18	0.01	K	179.14	1.59	177.65
8	0.60	0.06	0.16	0.01	K	179.30	0.88	178.78
9	1.77	0.16	0.22	0.03	K	180.23	1.59	178.55
10	0.49	0.05	0.06	0.00	K	177.95	0.51	177.55
11	0.81	0.07	0.10	0.01	K	180.36	1.16	179.64
12	0.14	0.03	0.23	0.02	K	176.96	0.07	176.90
13	0.10	0.03	0.24	0.02	K	177.68	0.31	177.67
14	0.26	0.02	0.21	0.02	K	176.94	0.02	176.77
15	0.70	0.06	0.11	0.01	K	180.64	1.25	180.03
16	0.82	0.07	0.20	0.02	K	178.94	1.04	178.21
17	0.23	0.02	0.13	0.01	K	176.46	0.62	176.32
18	0.88	0.08	0.20	0.02	K	176.80	−0.19	177.77
19	0.83	0.07	0.00	0.00	K	177.92	−0.58	178.84
20	0.49	0.00	0.13	0.00	S	177.02	−0.17	177.60
21	1.13	0.10	0.18	0.01	K	177.61	1.11	176.57
22	1.61	0.14	0.22	0.02	K	180.10	1.69	178.58
23	2.26	0.18	0.21	0.02	K	177.05	2.48	174.88
24	1.93	0.16	0.19	0.01	K	177.09	1.97	175.26
25	0.23	0.00	0.29	0.00	S	174.67	0.11	174.53
26	0.82	0.07	0.16	0.01	K	177.00	0.68	176.27
27	1.83	0.39	0.24	0.08	K	179.72	2.28	177.99
28	0.35	0.00	0.00	0.00	S	176.30	−0.52	176.75
29	1.02	0.10	0.30	0.02	K	177.28	−0.86	178.39
30	0.53	0.04	0.16	0.02	K	176.84	−0.75	177.46
31	0.04	0.00	0.25	0.00	S	178.68	0.37	178.76

Residue no.	$\lvert\Delta\omega_{N,MG}(^{13}CO)\rvert$*	Error*	$\lvert\Delta\omega_{N,I1}(^{13}CO)\rvert$*	Error*	Data quality*	ω_{CO}† pH 4.95, 35 °C	$\Delta\delta_{N,MG}$ (CO)‡ (pH 4.75, 35 °C)–(pH 4.1, 50 °C)	ω^{13CO}_{TrMG}§
32	0.54	0.09	0.37	0.03	K	177.69	−0.45	178.32
33	1.74	0.14	0.19	0.02	K	178.33	1.76	176.68
34	1.85	0.15	0.14	0.01	K	178.91	1.93	177.15
35	0.37	0.03	0.13	0.01	K	174.20	0.36	173.91
37	1.02	0.09	0.25	0.02	K	178.41	1.01	177.47
38	0.78	0.00	0.34	0.00	S	178.49	1.26	177.80
39	1.96	0.21	0.44	0.03	K	176.70	1.71	174.83
40	0.15	0.00	0.06	0.00	S	177.72	0.10	177.62
41	0.22	0.05	0.39	0.03	K	177.22	0.37	177.10
42	0.99	0.09	0.21	0.02	K	175.98	−0.72	177.07
43	0.15	0.02	0.29	0.02	K	176.57	0.75	176.51
44	1.02	0.00	0.30	0.00	S	175.63	−1.25	176.74
45	0.92	0.08	0.27	0.02	K	177.63	0.88	176.80
46	0.12	0.00	0.20	0.00	S	175.94	−0.12	176.06
48	0.02	0.00	0.24	0.00	S	174.69	0.13	174.75
49	2.00	0.16	0.16	0.01	K	175.47	−1.84	177.56
50	0.46	0.08	0.09	0.01	K	177.33	0.38	176.96
52	0.66	0.05	0.14	0.01	K	178.02	0.77	177.45
53	1.90	0.15	0.16	0.01	K	181.24	2.26	179.43
54	1.93	0.15	0.10	0.02	K	179.98	2.35	178.14
55	1.01	0.08	0.09	0.01	K	178.30	1.10	177.38
56	1.16	0.10	0.16	0.01	K	176.28	−0.85	177.54
57	1.11	0.09	0.13	0.01	K	177.65	−0.89	178.85
58	1.09	0.00	0.26	0.00	S	176.52	0.95	175.52
59	1.46	0.12	0.14	0.01	K	178.74	1.61	177.37
60	0.12	0.00	0.15	0.00	S	176.95	−0.44	177.18
61	0.32	0.03	0.12	0.01	K	178.23	−0.13	178.65
62	1.09	0.11	0.22	0.02	K	178.74	1.23	177.73
63	0.12	0.05	0.29	0.08	S	177.15	0.30	177.12
64	2.49	0.20	0.30	0.03	K	177.77	2.77	175.37
65	1.74	0.16	0.23	0.02	K	175.55	1.59	173.90
67	2.19	0.22	0.27	0.04	K	176.79	2.00	174.69
68	1.28	0.13	0.33	0.04	K	177.39	1.28	176.20
69	1.56	0.34	0.30	0.02	K	179.88	1.80	178.40
70	1.82	0.15	0.16	0.02	K	176.76	1.64	175.03
71	0.41	0.00	0.30	0.00	S	179.03	0.71	178.72
72	0.09	0.00	0.21	0.00	S	178.20	−0.04	178.40
73	0.02	0.00	0.27	0.00	S	174.60	−0.02	174.71
74	1.65	0.13	0.14	0.01	K	180.22	1.67	178.66
76	1.08	0.45	0.61	0.24	K	178.69	1.09	177.70
77	0.97	0.29	0.45	0.11	K	177.89	1.22	177.01
78	0.49	0.24	0.91	0.08	K	176.81	0.27	176.40
80	0.02	0.00	0.29	0.00	S	174.61	0.95	174.68
102	0.39	0.00	0.29	0.00	S	177.29	−0.60	177.76
104	0.18	0.00	0.16	0.00	S	177.51	−1.58	177.78
105	0.33	0.16	0.36	0.14	K	177.49	−0.14	177.92
106	2.05	0.00	0.42	0.00	S	179.79	2.43	177.83
107	0.34	0.07	0.32	0.05	K	177.61	0.63	177.36
108	0.91	0.20	0.44	0.11	K	176.32	0.72	175.50
109	0.54	0.04	0.19	0.01	K	178.90	0.85	178.45
110	1.01	0.08	0.15	0.01	K	179.23	−0.28	180.33
111	0.32	0.05	0.15	0.02	K	177.19	−0.14	177.60
112	0.18	0.02	0.21	0.02	K	177.73	0.06	177.65
113	0.94	0.08	0.11	0.01	K	178.74		177.89
114	0.62	0.05	0.14	0.01	K	177.76	0.56	177.24
115	0.72	0.06	0.09	0.01	K	178.33	0.26	177.70
116	0.93	0.08	0.19	0.01	K	175.73	1.02	174.89
117	2.25	0.18	0.21	0.02	K	176.52	2.28	174.35
118	0.89	0.07	0.11	0.01	K	176.85	1.21	176.06
120	2.55	0.20	0.30	0.02	K	179.92	2.51	177.46
121	0.20	0.00	0.28	0.00	S	174.51	0.52	174.39
122	1.67	0.14	0.15	0.01	K	174.67	−1.25	176.44
123	1.75	0.15	0.17	0.01	K	174.45	−1.61	176.29
124	0.81	0.07	0.19	0.01	K	173.42	−0.66	174.32
125	2.16	0.17	0.13	0.01	K	180.56	2.55	178.50
126	1.93	0.15	0.08	0.01	K	178.77	2.25	176.92
127	0.15	0.01	0.09	0.01	K	178.70	0.19	178.64
128	0.55	0.04	0.09	0.01	K	178.39	0.75	177.93
129	0.38	0.06	0.30	0.03	K	176.34	0.83	176.05
130	1.59	0.17	0.36	0.03	K	178.52	−0.75	180.20
131	0.72	0.14	0.13	0.01	K	178.02	0.79	177.39

Residue no.	$\lvert\Delta\omega_{N,MG}(^{13}CO)\rvert$*	Error*	$\lvert\Delta\omega_{N,I1}(^{13}CO)\rvert$*	Error*	Data quality*	ω_{CO}† pH 4.95, 35 °C	$\Delta\delta_{N,MG}$ (CO)‡ (pH 4.75, 35 °C)–(pH 4.1, 50 °C)	$\omega_{TrMG}^{^{13}CO}$§
132	0.94	0.20	0.26	0.03	K	178.54	1.14	177.69
133	0.16	0.04	0.25	0.02	K	178.43	0.31	178.36
134	0.27	0.11	0.65	0.05	K	179.47	0.33	179.28
135	0.27	0.00	0.28	0.00	S	179.07	0.41	178.89
136	0.16	0.00	0.42	0.00	S	178.83	0.44	178.76
137	1.33	0.23	0.19	0.04	K	179.82	1.23	178.58
138	0.73	0.16	0.24	0.03	K	176.13	−0.62	176.94
142	0.17	0.00	0.25	0.00	S	177.35	0.38	177.27
143	0.42	0.00	0.33	0.00	S	178.55	−0.61	179.06
144	2.11	0.57	0.34	0.05	K	177.67	−1.54	179.87
148	1.32	0.00	0.21	0.00	S	177.55	0.67	176.32
149	0.56	0.00	0.31	0.00	S	177.01	−0.42	177.66
150	0.19	0.04	0.33	0.03	K	174.04	0.10	173.93
151	0.12	0.07	0.21	0.02	K	175.55	0.16	175.52
152	0.43	0.07	0.34	0.05	K	174.63	−0.17	175.15

*Values of $\Delta\omega_{N,MG}$ and $\Delta\omega_{N,I1}$ (^{13}CO), and uncertainties in S-quality data were determined as described in Table S2; however, uncertainties for data of quality K were extracted from a 10,000-point grid search of the kinetic parameter space as described in the *SI Text*.

†ω_{CO} represents the (^{13}CO) chemical shift of native apoMb measured under identical sample conditions (pH 4.75, 35 °C) as the ^{13}CO relaxation dispersion data summarized in the table. Chemical shift assignments were acquired as described in *Materials and Methods*, and chemical shift referencing is indirectly based on DSS.

‡$\Delta\delta_{N,MG}$ is calculated as described in Table S2.

§$\omega_{TrMG}^{^{13}CO}$ is defined and calculated as described in Table S2, except for the sign of $\Delta\omega_{N,MG}$ (^{13}CO) of residue 113, which was set to that of $\Delta\delta_{N,MG}$ from the adjacent residues (112 and 114), because the MG state chemical shift for 113 is absent. The TALOS+ secondary structure predictions are unaffected by change in sign of $\Delta\omega_{N,MG}$ for residue 113.